Scientific Research Publishing

Journal of Applied Mathematics and Physics, 2022, 10, 1089-1097
https://www.scirp.org/journal/jamp
ISSN Online: 2327-4379
ISSN Print: 2327-4352

Tunable Optical Rotation with an *M*-Type Atomic System Using Vortex Beam

Zhenzhu Li

Department of Physics, University of Shanghai for Science and Technology, Shanghai, China
Email: lzz404505@163.com

How to cite this paper: Li, Z.Z. (2022) Tunable Optical Rotation with an *M*-Type Atomic System Using Vortex Beam. *Journal of Applied Mathematics and Physics*, **10**, 1089-1097.
https://doi.org/10.4236/jamp.2022.104075

Received: March 5, 2022
Accepted: April 8, 2022
Published: April 11, 2022

Copyright © 2022 by author(s) and Scientific Research Publishing Inc.
This work is licensed under the Creative Commons Attribution International License (CC BY 4.0).
http://creativecommons.org/licenses/by/4.0/

Open Access

Abstract

We consider the optical rotation of the polarization of a linearly polarized probe field passing through an *M*-type atomic system by using the interaction between two vortex control fields and optical transitions. We investigate theoretically to generate the spatially dependent structured light with the atoms acting as a spatially varying circular birefringent medium. We show that the polarization and intensity distributions of the vector beam spatially vary by changing the orbital angular momentum (OAM) of the vortex control field.

Keywords

Optical Rotation, Vortex Beam, Structured Light

1. Introduction

The coherent interaction of light with an atomic system has led to the investigation of many interesting phenomena in quantum optics and nonlinear optics [1] [2]. One important phenomenon is electromagnetic induced transparency (EIT) [3] caused by quantum interference, which can dramatically modify the optical response. In fact, EIT is essentially a destructive quantum interference effect between optical transitions; it creates a transparency window by eliminating a resonant absorption. As a result, EIT has been extensively investigated in many areas, such as multiwave mixing [4], optical solitons [5], and Kerr nonlinearity [6].

Recently, Radwell *et al.* [7] have demonstrated spatially dependent EIT for probe beam under the coherent controlling of OAM. Hamedi *et al.* [8] theoretically investigated the azimuthal modulation of EIT using vortex beam. The optical vortex beam can carry OAM, which provides an additional degree of free-

dom in the manipulation of the optical information, owing to its azimuthal coordinate and helical wavefront. It has established abundant prospects in the application, such as optical communications [9], optical manipulation [10], optical trapping [11], and atomic compass [12].

In this paper, the vortex beam is also used for coupling to generate the structured polarization between the applied fields, the induced vector beam is analyzed in terms of its propagation and polarization properties. Owing to the spatial susceptibility, the absorption of the components is the same, while dispersion is different. As a result, the spatial dispersion induces optical rotation and the probe field is vectored in the atomic medium. In addition, the polarization of the probe field can be modulated by adjusting the value of the magnetic field. The optical rotation makes the main contribution to generating the spatial vector beam. Optical rotation is crucial for the characterization of chiral molecules and is of importance to the study of pharmaceutical drugs, proteins, DNA, and many others, but their complex structure makes it difficult to analyze these effects from first principle. In our work, atoms serve as an easily characterized model to mimic this chiral interaction.

2. Theoretical Model and Formulation

We consider an M-type five-level atomic system [see Figure 1], which can be experimentally realized in cold atomic ^{87}Rb. The atoms are characterized by three ground states $|1\rangle=|5^2S_{1/2},F=2,m_F=-1\rangle$, $|2\rangle=|5^2S_{1/2},F=1,m_F=0\rangle$, $|3\rangle=|5^2S_{1/2},F=2,m_F=1\rangle$, $|4\rangle=|5^2P_{3/2},F=1,m_F=-1\rangle$ and $|4\rangle=|5^2P_{3/2},F=1,m_F=1\rangle$ are the degenerate upper states, which are generated by Zeeman shift due to a static magnetic field $\vec{B}=B\hat{z}$, $\Delta_B=g_F\mu_B B/\hbar$, g_F and μ_B are the *Landé* factor and Bohr magneton, respectively. A weak x-direction linearly polarized probe field $\vec{E}_p=\hat{x}\mathcal{E}_p\exp\left[-i\left(\omega_p t-k_p z\right)\right]+c.c.$ is composed of a right- and left-handed circularly polarized component, *i.e.*,

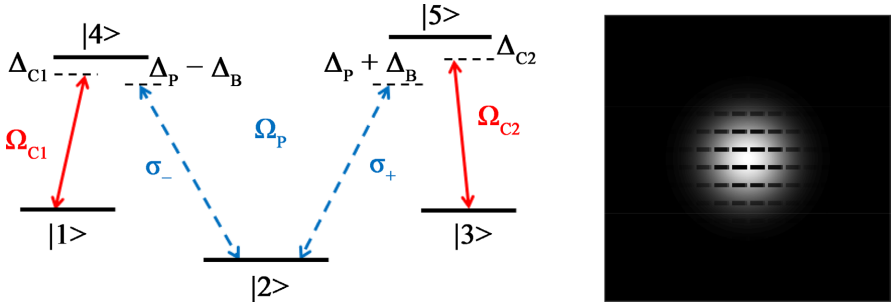

Figure 1. Schematic diagram of the M-type five-level system. A weak probe field with Rabi frequency Ω_p drives the transitions $|2\rangle\leftrightarrow|4\rangle$ and $|2\rangle\leftrightarrow|5\rangle$, with its σ_- polarization component and σ_+ polarization component, respectively. Two strong vortex control fields with Rabi frequencies Ω_{c1} and Ω_{c2} couple the transitions $|1\rangle\leftrightarrow|4\rangle$ and $|3\rangle\leftrightarrow|5\rangle$, respectively. The upper levels $|4\rangle$ and $|5\rangle$ are generated by the Zeeman shift, Δ_B. We denote with Δ_p, Δ_{c1}, and Δ_{c2} the one-photon detuning, respectively. The insets show the x-direction polarization profile of the initial probe light.

$\vec{E}_p = \left[\hat{\sigma}_- \mathcal{E}_{p-} + \hat{\sigma}_+ \mathcal{E}_{p+}\right] \exp\left[-i\left(\omega_p t - k_p z\right)\right] + c.c.$ drive respectively the transitions $|2\rangle \leftrightarrow |4\rangle$ and $|2\rangle \leftrightarrow |5\rangle$ with Rabi frequencies Ω_{p-} and Ω_{p+}, where $\Omega_{p-} = \left(\vec{\mu}_{42} \cdot \hat{\sigma}_{p-}\right)\mathcal{E}_{p-}/\hbar$, $\Omega_{p+} = \left(\vec{\mu}_{52} \cdot \hat{\sigma}_{p+}\right)\mathcal{E}_{p+}/\hbar$, $\mathcal{E}_{p\pm} = \mathcal{E}_p/\sqrt{2}$ are the slowly varying envelopes, $\hat{\sigma}_- = \left(\hat{x} - i\hat{y}\right)/\sqrt{2}$ and $\hat{\sigma}_+ = \left(\hat{x} + i\hat{y}\right)/\sqrt{2}$ are the unit vectors of the orthogonal polarization components, and $|\vec{\mu}_{42}| = |\vec{\mu}_{52}| = |\vec{\mu}|$. Also, two π-polarized vortex control fields $\vec{E}_{c1} = \hat{x}\mathcal{E}_{c1} \exp\left[-i\left(\omega_{c1} t - k_{c1} z\right)\right] + c.c.$ and $\vec{E}_{c2} = \hat{x}\mathcal{E}_{c2} \exp\left[-i\left(\omega_{c2} t - k_{c2} z\right)\right] + c.c.$ excite the transitions $|1\rangle \leftrightarrow |4\rangle$ and $|3\rangle \leftrightarrow |5\rangle$ with Rabi frequencies $\Omega_{c1} = \left(\vec{\mu}_{41} \cdot \hat{\sigma}_{c1}\right)\mathcal{E}_{c1}/\hbar$ and $\Omega_{c2} = \left(\vec{\mu}_{53} \cdot \hat{\sigma}_{c2}\right)\mathcal{E}_{c2}/\hbar$, respectively. Here, $\hat{\sigma}_{c1}$ and $\mathcal{E}_{c1}$ ($\hat{\sigma}_{c2}$ and $\mathcal{E}_{c2}$) are the unit vector and the slowly varying envelope of the control field. Moreover, μ_{ij} is the dipole moment corresponding to $|i\rangle \leftrightarrow |j\rangle$ transition.

Under the rotating-wave approximation, the time-independent Hamiltonian of the system is written as:

$$\begin{aligned} H = \hbar\Big[&\left(\Delta_p - \Delta_B - \Delta_{c1}\right)|1\rangle\langle 1| + \left(\Delta_p + \Delta_B - \Delta_{c2}\right)|3\rangle\langle 3| \\ &+ \left(\Delta_p - \Delta_B\right)|4\rangle\langle 4| + \left(\Delta_p + \Delta_B\right)|5\rangle\langle 5|\Big] \\ &- \hbar\left(\Omega_{c1}|4\rangle\langle 1| + \Omega_{c2}|5\rangle\langle 3| + \Omega_{p-}|4\rangle\langle 2| + \Omega_{p+}|5\rangle\langle 2| + H.c.\right), \end{aligned} \tag{1}$$

where $\Delta_p = \omega_p - \omega_{42} - \Delta_B$, $\Delta_{c1} = \omega_{c1} - \omega_{41}$ and $\Delta_{c2} = \omega_{c2} - \omega_{53}$ are the one-photon resonance detunings, respectively.

The dynamics of the atomic population can be calculated by the Liouville equation:

$$\dot{\rho} = -\frac{i}{\hbar}[H, \rho] + \Gamma\rho, \tag{2}$$

The second term in Equation (2) represents radiative processes that can be expressed as:

$$\Gamma\rho = -\sum_{i=4}^{5}\sum_{j=1}^{3}\frac{\gamma_{ij}}{2}\left(|i\rangle\langle i|\rho - 2|j\rangle\langle j|\rho_{ii} + \rho|i\rangle\langle i|\right), \tag{3}$$

where γ_{ij} represents radiative decay rates from excited states $|i\rangle$ to ground states $|j\rangle$ and γ_c is the collision rate. The dynamics of the density matrix equations can be obtained by substituting the Hamiltonian Equation (1) into the Liouville equation Equation (2):

$$\dot{\rho}_{11} = i\left(\Omega_{c1}^*\rho_{41} - \Omega_{c1}\rho_{14}\right) + \gamma_{41}\rho_{44} + \gamma_{51}\rho_{55},$$

$$\dot{\rho}_{22} = i\left(\Omega_{p-}^*\rho_{42} - \Omega_{p-}\rho_{24} + \Omega_{p+}^*\rho_{52} - \Omega_{p+}\rho_{52}\right) + \gamma_{42}\rho_{44} + \gamma_{52}\rho_{55},$$

$$\dot{\rho}_{33} = i\left(\Omega_{c2}^*\rho_{53} - \Omega_{c2}\rho_{35}\right) + \gamma_{43}\rho_{44} + \gamma_{53}\rho_{55},$$

$$\dot{\rho}_{44} = i\left(\Omega_{c1}\rho_{14} - \Omega_{c1}^*\rho_{41} + \Omega_{p-}\rho_{24} - \Omega_{p-}^*\rho_{42}\right) - \gamma\rho_{44},$$

$$\dot{\rho}_{31} = i\left[\Omega_{c2}^*\rho_{51} - \Omega_{c1}\rho_{34} - \left(2\Delta_B + \Delta_{c1} - \Delta_{c2}\right)\rho_{31}\right],$$

$$\dot{\rho}_{41} = i\left[\Omega_{c1}\left(\rho_{11} - \rho_{44}\right) + \Omega_{p-}\rho_{21} - \Delta_{c1}\rho_{41}\right] - \frac{\gamma}{2}\rho_{41},$$

$$\dot{\rho}_{51} = i\left[\Omega_{p+}\rho_{21} + \Omega_{c2}\rho_{31} - \Omega_{c1}\rho_{54} - \left(2\Delta_B + \Delta_{c1}\right)\rho_{51}\right] - \frac{\gamma}{2}\rho_{51},$$

$$\dot{\rho}_{12} = i\left[\Omega_{c1}^{*}\rho_{42} - \Omega_{p-}\rho_{14} - \Omega_{p+}\rho_{15} - \left(\Delta_p - \Delta_B - \Delta_{c1}\right)\rho_{12}\right],$$

$$\dot{\rho}_{32} = i\left[\Omega_{c2}^{*}\rho_{52} - \Omega_{p-}\rho_{34} - \Omega_{p+}\rho_{35} - \left(\Delta_p + \Delta_B - \Delta_{c2}\right)\rho_{32}\right],$$

$$\dot{\rho}_{42} = i\left[\Omega_{c1}\rho_{12} + \Omega_{p-}\left(\rho_{22} - \rho_{44}\right) - \Omega_{p+}\rho_{45} - \left(\Delta_p - \Delta_B\right)\rho_{42}\right] - \frac{\gamma}{2}\rho_{42},$$

$$\dot{\rho}_{52} = i\left[\Omega_{p+}\left(\rho_{22} - \rho_{55}\right) + \Omega_{c2}\rho_{32} - \Omega_{p-}\rho_{54} - \left(\Delta_p + \Delta_B\right)\rho_{52}\right] - \frac{\gamma}{2}\rho_{52},$$

$$\dot{\rho}_{43} = i\left[\Omega_{c1}\rho_{13} + \Omega_{p-}\rho_{23} - \Omega_{c2}\rho_{45} - \left(\Delta_{c2} - 2\Delta_B\right)\rho_{43}\right] - \frac{\gamma}{2}\rho_{43},$$

$$\dot{\rho}_{53} = i\left[\Omega_{p+}\rho_{23} + \Omega_{c2}\left(\rho_{33} - \rho_{55}\right) - \Delta_{c2}\rho_{53}\right] - \frac{\gamma}{2}\rho_{53},$$

$$\dot{\rho}_{54} = i\left[\Omega_{p+}\rho_{24} - \Omega_{c1}^{*}\rho_{51} - \Omega_{p-}^{*}\rho_{52} + \Omega_{c2}\rho_{34} - 2\Delta_B\rho_{54}\right],$$

$$\dot{\rho}_{55} = -\left(\dot{\rho}_{11} + \dot{\rho}_{22} + \dot{\rho}_{33} + \dot{\rho}_{44}\right), \tag{4}$$

where $\dot{\rho}_{ji} = \dot{\rho}_{ij}^{*}$. Assuming $\gamma_{41} = \gamma_{42} = \gamma_{43} = \gamma_{51} = \gamma_{52} = \gamma_{53} = \frac{\gamma}{3}$, here the γ is the spontaneous decay rate of excited states.

We further assume that the atom is initially prepared in the ground state $|2\rangle$, *i.e.*, $\rho_{22} = 1$. Consequently, we obtain the following off-diagonal density-matrix elements:

$$\rho_{42} = -\frac{i\xi_3\Omega_{p-}}{\xi_1\xi_3 + \left|\Omega_{c1}\right|^2},$$

$$\rho_{52} = -\frac{i\xi_4\Omega_{p+}}{\xi_2\xi_4 + \left|\Omega_{c2}\right|^2}, \tag{5}$$

where $\xi_1 = -i\left(\Delta_p - \Delta_B\right) - \gamma/2$, $\xi_2 = -i\left(\Delta_p + \Delta_B\right) - \gamma/2$, $\xi_3 = -i\left(\Delta_p - \Delta_B - \Delta_{c1}\right)$, and $\xi_4 = -i\left(\Delta_p + \Delta_B - \Delta_{c2}\right)$.

The susceptibility of the induced medium corresponding to the right- and left-handed circularly polarized components of the probe field is given by:

$$\chi_{-} = \frac{\mathcal{N}\left|\vec{\mu}\right|^2\rho_{42}}{\varepsilon_0\hbar\Omega_{p-}},$$

$$\chi_{+} = \frac{\mathcal{N}\left|\vec{\mu}\right|^2\rho_{52}}{\varepsilon_0\hbar\Omega_{p+}}, \tag{6}$$

where $\mathcal{N}$ and ε_0 are the atomic density and vacuum permittivity of the medium, respectively. The imaginary and real parts of $\chi_{\pm}$ represent the absorption and dispersion for the left and right circular polarization components of the probe field. The difference in the real part of the susceptibility, *i.e.*, $\chi_{\pm}$, results in inducing the circular birefringence. Subsequently, induced circular birefringence causes the rotation as the polarization plane of the probe light passing through the medium. However, the difference of imaginary part of the $\chi_{\pm}$ leads to circular dichroism and linearly probe light evolves into elliptically polarized light.

To study the spatially dependent optical activity, we assume the both control fields with Rabi frequencies Ω_{c1} and Ω_{c2} carry optical vortices:

$$\Omega_n = \Omega_{n0}\left(\frac{r\sqrt{2}}{w_c}\right)^{|l_n|}\exp\left(-\frac{r^2}{w_c^2}\right)\exp\left(il_n\phi\right), \tag{7}$$

where Ω_n, and l_n ($n\in\{c1,c2\}$) are the amplitude, topological charge. Here w_c is the beam waist at $z=0$. We define $r=\sqrt{x^2+y^2}$ and $\phi=\tan^{-1}\left(y/x\right)$ as the distance from the center of the core and the azimuthal angle.

3. Results and Discussions

Throughout this paper, all the parameters are scaled by $\gamma=2\pi\times10$ MHz. Here, we first investigate the influence of OAM carried by the vortex beams on the absorption and dispersion corresponding to the right- and left-handed circularly polarized components of the transmitted probe, as depicted in one-dimension x in Figure 2, for different topological charge, *i.e.*, $l_{c1}=l_{c2}=l$. It is shown that the absorption of the circular orthogonal components of the probe field is approximately the same and circular dichroism would be ignored, while the

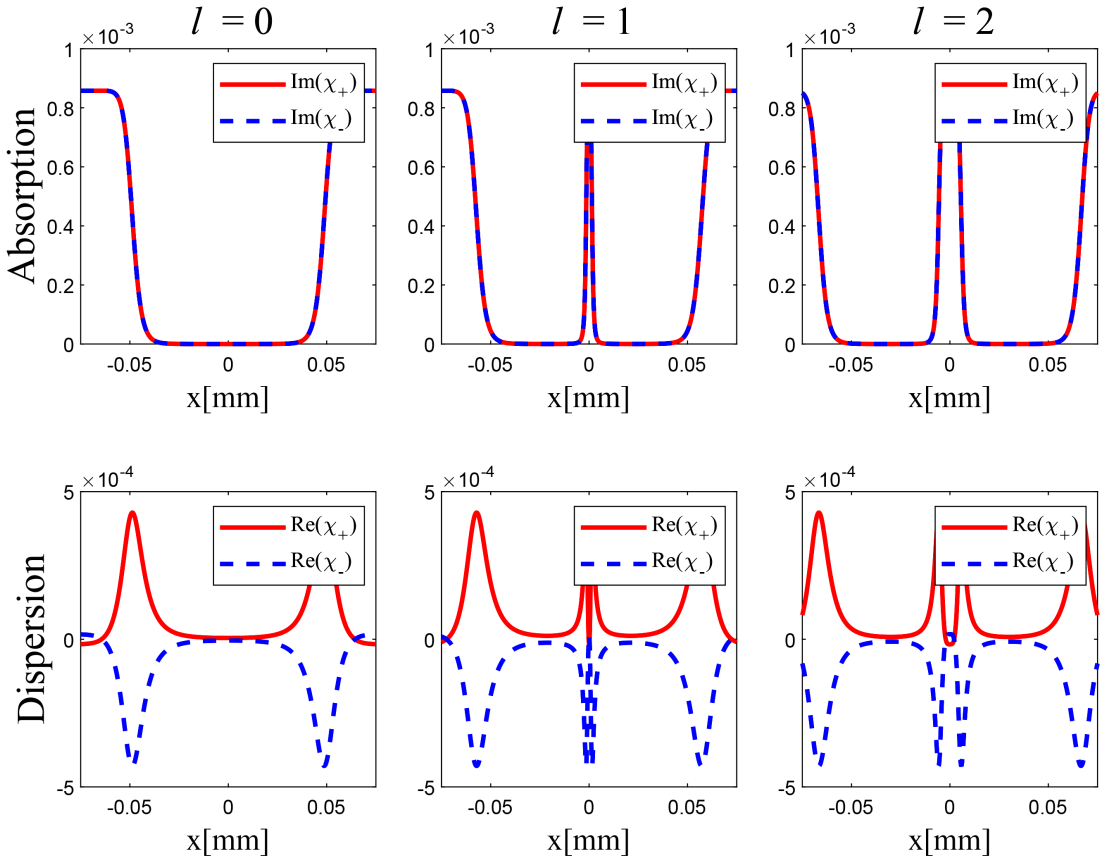

Figure 2. The absorption and dispersion of the $\chi_{\pm}$ for different topological charge in x-dimension. All parameters are scaled by $\gamma=2\pi\times$ MHz. In order to satisfy the perturbation condition, we choose the parameters as $\mathcal{N}=2\times10^{10}\,\text{atoms}/\text{cm}^3$, $L=60\,\mu\text{m}$, $w_p=30\,\mu\text{m}$, $\lambda_p=780\,\text{nm}$, $\Omega_{p-}=0.01\gamma$, $\Omega_{p+}=0.01\gamma$, $\Omega_{c10}=\gamma$, $\Omega_{c20}=\gamma$, $\Delta_p=\Delta_{c1}=\Delta_{c2}=0$, $\Delta_B=0.01\gamma$.

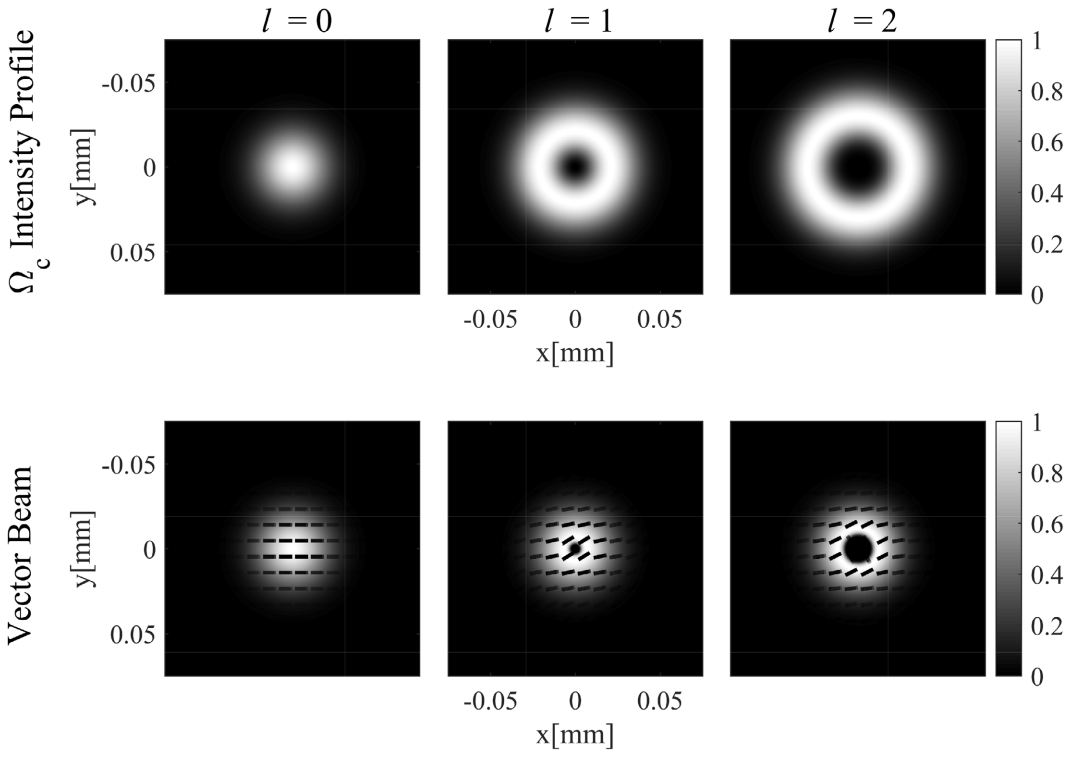

Figure 3. Intensity profile of the vortex control fields (first row), and the spatial polarization distribution and intensity profile of the transmitted probe light (second row) for different topological charge. Other parameters are the same as those in **Figure 2**.

dispersion of the right- and left-circular components is different in sign, which leads to inducing the spatially circular birefringence and further generates the beam with the spatially dependent polarization. Moreover, there is only two absorption peak when $l = 0$ and three peaks for $l \neq 0$, and the center of absorption peak is accompanied by an increase in l.

In the following, we investigate the effect of the vortex beams on the rotation of the polarization plane of linearly probe field in the transverse section of the transmitted profile. **Figure 3** shows the intensity profile of the vortex control fields (first row), and the spatial polarization distribution and intensity profile of the transmitted probe light (second row) for different topological charges. When the $l \neq 0$, it can be seen from **Figure 3** that the Gaussian intensity profile of the probe field evolves into the doughnut shape after transmission of the atomic system, and the *x*-direction linearly polarization distribution becomes a vector beam at the output $z = L$. It should be noted that the resulting vector beam experiences the spatially optical rotation at different transverse profile of the transmitted probe field, and the optical rotation angle θ is defined as $\theta = k_p\left[Re(\chi_+) - Re(\chi_-)\right]/2$. It can also be seen from **Figure 3** that the optical rotation near the center is the most obvious, which coincides with the region with the largest dispersion difference in **Figure 2**. Thus, the observed optical rotation is caused by the difference of the dispersion of the orthogonal polarization components of the probe field. In addition, the generation of vector beam de-

pends on the topological charge of the vortex control fields.

We then consider the effect of different Zeeman shift, Δ_B, on the absorption and dispersion of correspond to probe field in the presence of both vortex control beams, under the topological charge $l=1$. Figure 4 shows that with the Δ_B from 0.01γ to 0.1γ, the absorption peak in the central region widens, and the central becomes transparent at $\Delta_B=\gamma$, however two new absorption peaks arise around it. Meanwhile, the dispersion is still a mirror model and the two peaks in the center gradually separate from each other as Δ_B increases, the change of Δ_B does not affect the formation of structured light, in contrast, it plays a vital important on the spatially-dependent polarization profile of the vector beam. Clearly, using the magnetic field can modulate the absorption of the induced medium to the probe light, so as to obtain the expected shape of structured light.

We have demonstrated that the spatially dependent polarization profile is sensitively on the dispersion in the case of resonance. Applying different Δ_B generates the various the dispersion. In order to give a more comprehensive description dynamic polarization of the transmitted probe field in Figure 4, we show the polarization distribution and intensity profile of the transmitted field in Figure 5. It can be found that the shape of vector depends on the Δ_B, this result

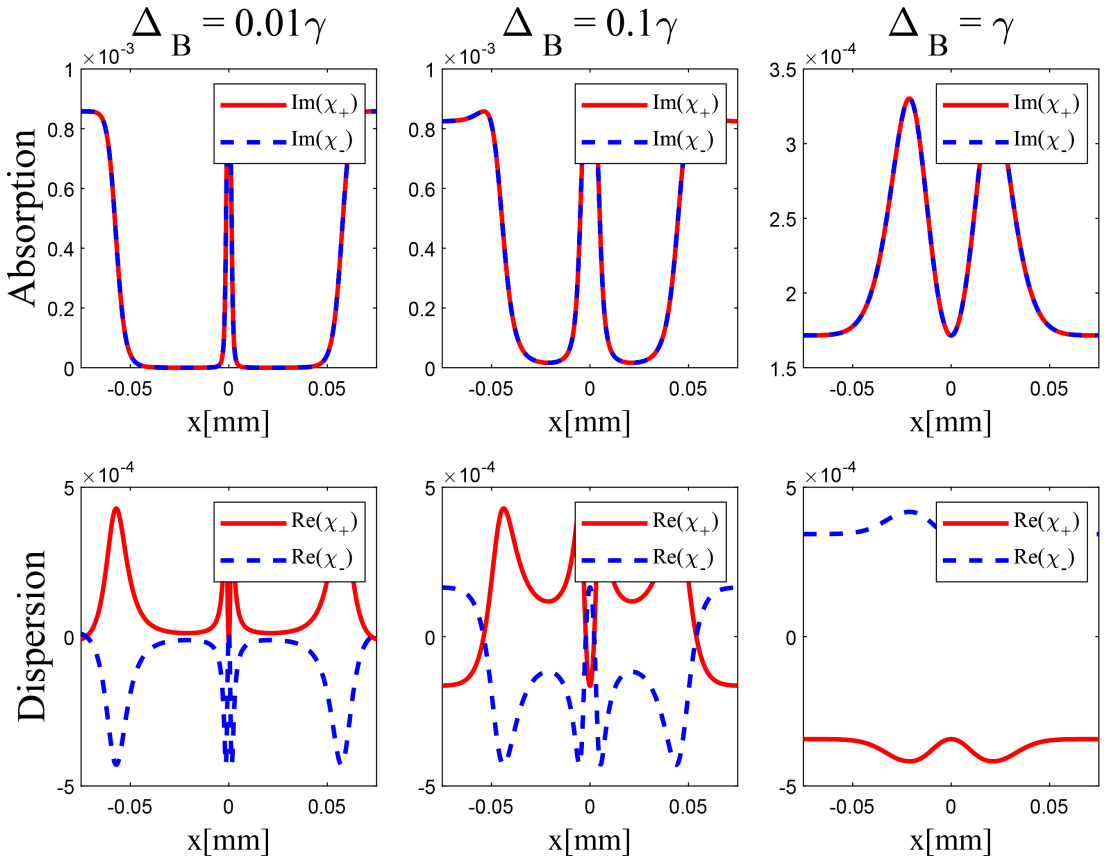

Figure 4. The absorption and dispersion of the $\chi_{\pm}$ for different Δ_B in x-dimension and $l=1$. Other parameters are the same as those in Figure 2.

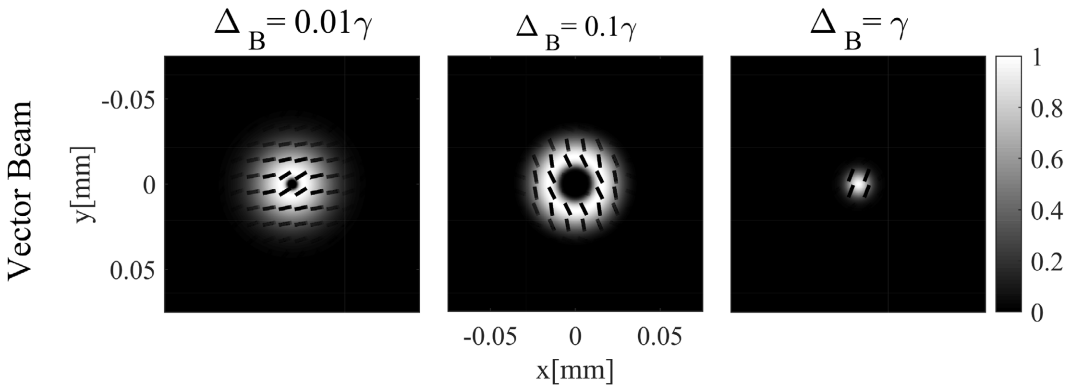

Figure 5. The spatial polarization distribution and intensity profile of the transmitted probe light for different Δ_B. Other parameters are the same as those in **Figure 2**.

is in agreement with that shown in **Figure 4**. It is worth noting that an increase in Δ_B leads to an increase in absorption loss, and the ring of transmitted probe light becomes narrow. Similarly, the spatial distribution of the polarization is completely identical in **Figure 4**. These properties of the susceptibility are the result of the interaction between the vortex beam and the atomic system as well as the destructive quantum interference generated by the two optical vortices under resonance conditions.

4. Conclusion

In summary, the linear susceptibility of the weak probe field depends on the azimuthal angle and OAM of the control beams and in turn affects the shape and polarization of the transmitted probe light spatially. We find that the induced optical rotation plays an important role in the generation of vector beam. In addition, we found that the shape of the intensity of the vector beam can be easily controlled by the characteristics of the vortex control field and magnetic field. Our work provides a simple generation method for controllable spatial distribution and intensity of vector beam, improving capacity storage in optical communication.

Conflicts of Interest

The author declares no conflicts of interest regarding the publication of this paper.

References

[1] Boller, K.J., Imamoğlu, A. and Harris, S.E. (1991) Observation of Electromagnetically Induced Transparency. *Physical Review Letters*, **66**, 2593. https://doi.org/10.1103/PhysRevLett.66.2593

[2] Kang, H. and Zhu, Y. (2003) Observation of Large Kerr Nonlinearity at Low Light Intensities. *Physical Review Letters*, **91**, Article ID: 093601. https://doi.org/10.1103/PhysRevLett.91.093601

[3] Agarwal, G.S. and Huang, S. (2010) Electromagnetically Induced Transparency in

Mechanical Effects of Light. *Physical Review A*, **81**, Article ID: 041803. https://doi.org/10.1103/PhysRevA.81.041803

[4] Wang, Z., Zhang, Y., Paspalakis, E., *et al.* (2020) Efficient Spatiotemporal-Vortex Four-Wave Mixing in a Semiconductor Nanostructure. *Physical Review A*, **102**, Article ID: 063509. https://doi.org/10.1103/PhysRevA.102.063509

[5] Chen, Y., Chen, Z. and Huang, G. (2015) Storage and Retrieval of Vector Optical Solitons via Double Electromagnetically Induced Transparency. *Physical Review A*, **91**, Article ID: 023820. https://doi.org/10.1103/PhysRevA.91.023820

[6] Hamedi, H.R., Yannopapas, V., Mekys, A., *et al.* (2021) Control of Kerr Nonlinearity in a Four-Level Quantum System near a Plasmonic Nanostructure. *Physica E: Low-Dimensional Systems and Nanostructures*, **130**, Article ID: 114662. https://doi.org/10.1016/j.physe.2021.114662

[7] Radwell, N., Clark, T.W., Piccirillo, B., *et al.* (2015) Spatially Dependent Electromagnetically Induced Transparency. *Physical Review Letters*, **114**, Article ID: 123603. https://doi.org/10.1103/PhysRevLett.114.123603

[8] Hamedi, H.R., Kudriaov, V., Ruseckas, J., *et al.* (2018) Azimuthal Modulation of Electromagnetically Induced Transparency Using Structured Light. *Optics Express*, **26**, 28249-28262. https://doi.org/10.1364/OE.26.028249

[9] El-Meadawy, S.A., Farghal, A.E.A., Shalaby, H.M.H., *et al.* (2021) Efficient and Secure Bit-Level Chaos Security Algorithm for Orbital Angular Momentum Modulation in Free-Space Optical Communications. *IEEE Access*, **9**, 74817-74835. https://doi.org/10.1109/ACCESS.2021.3074894

[10] Shen, Y., Wang, X., Xie, Z., *et al.* (2019) Optical Vortices 30 Years on: OAM Manipulation from Topological Charge to Multiple Singularities. *Light: Science and Applications*, **8**, 1-29. https://doi.org/10.1038/s41377-019-0194-2

[11] Hui, X., Zheng, S., Chen, Y., *et al.* (2015) Multiplexed Millimeter Wave Communication with Dual Orbital Angular Momentum (OAM) Mode Antennas. *Scientific Reports*, **5**, 1-9. https://doi.org/10.1038/srep10148

[12] Castellucci, F., Clark, T.W., Selyem, A., *et al.* (2021) Atomic Compass: Detecting 3D Magnetic Field Alignment with Vector Vortex Light. *Physical Review Letters*, **127**, Article ID: 233202. https://doi.org/10.1103/PhysRevLett.127.233202